

Slender Object Detection: Diagnoses and Improvements

Zhaoyi Wan^{1*}; Yimin Chen^{2*}; Sutaο Deng^{2*}; Cong Yao³, Jiebo Luo¹,
¹University of Rochester, ²Beihang University, ³Megvii
i@wanzy.me, jluo@cs.rochester.edu

Abstract

*In this paper, we are concerned with the detection of a particular type of objects with extreme aspect ratios, namely **slender objects**. In real-world scenarios as well as widely-used datasets (such as COCO), slender objects are actually very common. However, this type of objects has been largely overlooked by previous object detection algorithms. Upon our investigation, for a classical object detection method, a drastic drop of 18.9% mAP on COCO is observed, if solely evaluated on slender objects. Therefore, We systematically study the problem of slender object detection in this work. Accordingly, an analytical framework with carefully designed benchmark and evaluation protocols is established, in which different algorithms and modules can be inspected and compared. Our key findings include: 1) the essential role of anchors in label assignment; 2) the descriptive capability of the 2-point representation; 3) the crucial strategies for improving the detection of slender objects and regular objects. Our work identifies and extends the insights of existing methods that are previously underexploited. Furthermore, we propose a feature adaption strategy that achieves clear and consistent improvements over current representative object detection methods. In particular, a natural and effective extension of the center prior, which leads to a significant improvement on slender objects, is devised. We believe this work opens up new opportunities and calibrates ablation standards for future research in the field of object detection.*

1. Introduction

As a fundamental task in computer vision that draws considerable research attention from the community, object detection [6, 22, 21] has made substantial progress in recent years. As the needs of real-world applications in a wide variety of scenarios arise [31, 24], the significance of research regarding a particular topic elevates. The works on improving specific aspects [11, 33] of object detection, such as detecting dense objects [5, 12] and small objects [34], boost

Table 1: $mAP(\%)$ gap between tall and wide objects on COCO. Objects are grouped by the width/height ratio r_b of bounding boxes, where XT=extra tall; T=tall; M=medium; W=wide; XW=extra wide, as defined by [10].

| Method | all | XT | T | M | W | XW |
|-----------|------|------|------|------|------|------|
| RetinaNet | 36.4 | 19.2 | 26.8 | 38.1 | 24.6 | 12.7 |
| Faster | 37.9 | 23.3 | 31.4 | 39.0 | 26.1 | 16.8 |

the practical value of object detection and consequently inspire further advances [2, 7].

While a large portion of the problems have been well investigated and numerous new ideas have been proposed, grand challenges remained in object detection. [18] propose the focal loss to tackle dense object detection and prompt it to become a common practice for classification loss in object detection.

Object scale has been widely considered in model design, as various detection paradigms [6], augmentation schemes [34], and modules [1] are proposed to improve small object detection. Such insightful works propel object detection methods to transfer from academic research to a wide variety of real-world applications [27, 16]. Despite such progress in object detection, one significant problem has not been formally explored in previous works.

This work is dedicated to studying the problem of slender object detection. From the perspective of academic research, the distinctive properties of slender objects pose special challenges, which give rise to research topics of scientific value. From the perspective of application, once slender objects can be well-handled, the practical utility of object detection systems will become higher.

Inspired by previous works [10, 8, 14], which provide in-depth ablations, analyses, and insights regarding object detection algorithms, we start with diagnosing and analyzing existing methods for object detection. Specifically, we establish a unified analytical framework, which includes the formal definition of slender objects, a standardized pipeline for object detection, and a new benchmark dataset and corresponding evaluation protocols. With the proposed framework, different object detection methods can be dissected

* Authors contribute equally

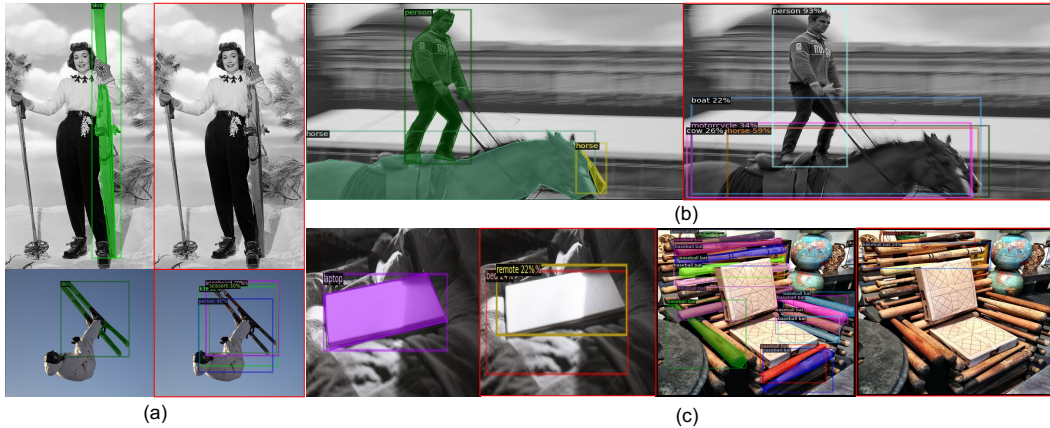


Figure 1: Slender object examples. Images marked with red borders visualize detection results. The ski in the top left is missed by the detector due to anchor mismatching.

and compared in a clear and fair manner. In addition, it is convenient to identify the key factors (such as critical components and effective choices) for the success of previous methods, reveal the limitations of previous methods, and more importantly, discover potential directions for improving slender object detection. Key findings relate to the role of anchors, the capability of the 2-point representation, and the effect of feature adaption, as well as more details and discussions, are presented in Sec. 3.

Beyond diagnoses and analyses, we further propose strategies to boost the detection of slender objects. In particular, a generalized feature adaption module, called self-adaption, is introduced. In addition, we extend the center prior (originated from FCOS [26]) to slenderness prior to adapt to the nature of slender objects. According to the quantitative experiments (see Sec. 4), these two components have proven effective for slender objects while also working well for regular objects. Our recommended combinations can match or even outperform previous state-of-the-art methods on COCO (see Fig. 7).

In summary, the contributions of this paper are as follows:

- We are the first to formally investigate the problem of slender object detection, which is important but largely overlooked by previous works.
- We construct an analytical framework for rigorously diagnosing different object detection methods. With this framework, a series of key insights and valuable findings, which may inspire other researchers in the field of object detection, is derived.
- We identify the feature adaption module as a key factor for the excellent performance of previous methods. A generalized feature adaption module, called self-adaption, is devised. Our experiments indicate that the self-adaption module is both effective and general.
- We extend the center prior to slenderness prior, which



Figure 2: Slenderness estimation from bounding box (red) and oriented box (green).

significantly improves the performance on slender objects.

2. Preliminary Assessment

In this section, we will provide an overview of slender object detection and conduct a preliminary assessment on existing methods. As shown in Fig. 1, slender objects in images can be roughly categorized into three groups: **Distinct slender objects** are those that are intrinsically slender in shape, such as ski, forks, and bats. **Regular objects** may also appear slender in images because of **occlusion and truncation** (top right in Fig. 1). In addition, some **thin plates** in the real world may appear slender from certain viewing angles, e.g., books and tables. Different categories of objects exhibit different characteristics but may also share some properties in common. We analyze typical errors by previous methods for these different categories, and accordingly draw unified conclusions regarding slender objects.

2.1. Definition and Evaluation Protocols

For targeted evaluation and analyses, we need to estimate the slenderness of objects. In the context of object detection where bounding boxes are the common representation of objects, slenderness can be approximately computed from the width w_b and height h_b of axis-aligned bounding boxes as $r_b = w_b/h_b$. This formula is specifiable for both the ground truth and detection results, thus being fully applicable to existing evaluation protocols, e.g., mAP and mAR. However, the deviation of r_b is obviously inaccurate for oriented slender objects as illustrated in Fig. 3. It would mistake oriented slender objects as regular objects and in consequence underestimate the gap between regular and slender objects. The more accurate approach is to find a rotated box which covers the object with the minimal area (green box in Fig. 3 top left), and compute the slenderness s as:

$$s = \min(w, h) / \max(w, h). \quad (1)$$

w and h are the width and height of the minimum-area rectangle. For the convenience of comparison, we refer to objects with $s < 1/5$, $1/5 < s < 1/3$, $s > 1/3$ as extra slender (XS), slender (S), and regular (R), respectively.

Meanwhile, particular mAP can not be precisely computed in this estimation. The slenderness of false positives is undefined as the detection results are still bounding boxes. Therefore, we use mAR as the metric for particularly benchmarking slender object detection in this work, since it does not need to identify the number of false positives but limits the amount of detection in an image. We refer readers not familiar with the computation of mAP and mAR to Appendix A in the supplementary material for a detailed explanation.

2.2. Data Bias Neutralization

As mentioned above, we rely on precise boundaries of objects to estimate their slenderness, which is not feasible with conventional axis-aligned bounding box annotations in object detection. Fortunately, the COCO dataset [19], one of the most popular datasets in recent research of object detection, provides pixel-level segmentation labels. COCO is a large-scale dataset collected for object detection and related tasks, e.g., keypoint detection and panoptic segmentation. For object detection, it contains more than 200k images in the 2017 release, where 118k images are labeled for training and the other 5k images are kept as a validation set.

However, COCO is biased regarding slender objects and not sufficient for evaluating slender object detection by itself. The data distribution of COCO is visualized in Fig. 3, where more than 85% of objects are regular. The dominant proportion in the dataset implicitly forces the current evaluation to favor regular objects over slender objects. As shown in Fig. 4, the overall mAR in COCO is close to that

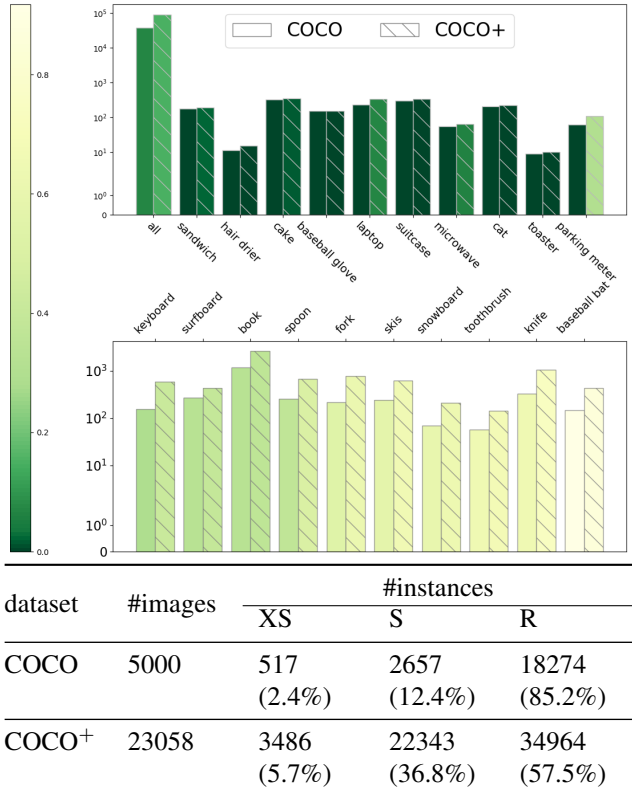


Figure 3: Number of instances of different object categories in COCO and COCO+ validation set. Clearly COCO+ is more neutralized in terms of slenderness.

of regular objects. Such a bias against slender objects can be mitigated by extending the validation set of COCO.

We incorporate slender objects from another dataset, Objects365 [25], to complement COCO. Objects365 is a dataset aiming at object detection in the wild, containing 38k validation images sharing similar characteristics with COCO. In contrast to COCO which provides detailed boundaries of objects, Objects365 annotates objects with axis-aligned bounding boxes. We use a top-performing instance segmentation model by [2] with a ResNeXt152 [30] backbone to generate polygon borders of objects. Given ground truth bounding boxes during inference, the produced masks are accurate for slenderness estimation. The procedure and examples of polygon generation are shown in Appendix B in the supplementary material. According to the slenderness estimated from generated borders, we select images containing extra slender objects in Objects365 to mix with the COCO validation set, creating COCO+. As shown in Fig. 3, the number of slender objects in COCO+ is 8 times more than COCO, thus mitigating the bias against slender objects. Experimental validation shown in Fig. 4 verifies that COCO+ is fairly balanced since the overall mAR is closer to the average of mAR on extra slender objects and mAR of regular objects.

2.3. Error Analysis

Using the evaluation protocols and data mentioned above, we assess the problem by comprehensively evaluating a representative method [18]. Models we implemented in this paper are built upon a ResNet50 [9] backbone with FPN [17] and trained on the COCO training set with a 1x schedule. To keep the experiments directly comparable to the literature, we also provide evaluation results on COCO mAP. The evaluation results are shown in Fig. 4.

It is noteworthy that detection mAR is inversely proportional to object slenderness, with a gap of 19.3% between XS and R objects. This correlation is consistent with different data sets, IoU thresholds, and object areas. For lower thresholds (< 0.7), the performance drop of extra slender objects is more significant. Since lower thresholds tolerate inaccurate localization results more, this phenomenon indicates that it is more difficult to accurately classify slender objects. In consideration of the notable overlap between slender and small objects, we separately evaluate objects with different areas. As shown in the last row of Fig. 4, mAR on slender objects are consistently worse than regular objects with a large gap, regardless of the area of objects. The gap is more significant for large objects, due to the increase of challenges in estimating object sizes.

An intuitive alleviation of the problems on slender object detection is to increase the sample rate of slender objects in the dataset during training, and the results are shown in Tab. 2. It demonstrates the change of sampling rate in the training data as a trade-off between the effectiveness on regular and slender objects. Accompanying the increase of slender and extra slender mAR, the regular mAR drops. What we concern more is that, when the sample rates of slender objects continue to increase, the drop of overall performance is also escalated. Therefore, besides data sampling, further investigation is warranted to find truly effective solutions.

In addition to quantitative comparisons, qualitative visualization of typical errors is given in Fig. 1. One of the major errors is caused by the mismatch of regular shape anchors and the slender shape of objects, as shown in Fig. 1a. Vertical and horizontal slender objects can be improperly assigned by the IoU matching between the bounding box and pre-defined anchors during training. As for oriented slender objects, false positives introduced by improper IoU matching hinder effective duplication removal. As mentioned above, regular objects may appear slender in images because of occlusion, which may cause false classifications by the detectors. An example is shown in Fig. 1b in which those dense predictions at different locations result in different classifications. The false detection can not be removed by regular NMS (non-maximum suppression) because of their different predicted classes. Another group of slender objects such as books and forks often appears in clusters

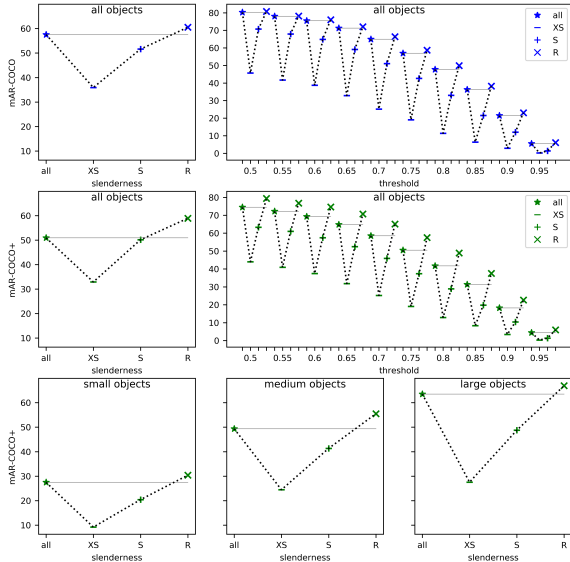


Figure 4: Despite across-the-board performance drop on slender objects, COCO+ is fairly balanced.

Table 2: RetinaNet with different sampling rates during training.

| sample rate | | | COCO+ mAR | | | | COCO mAP |
|-------------|---|---|-----------|------|------|------|----------|
| XS | S | R | all | XS | S | R | |
| 1 | 1 | 1 | 48.4 | 24.0 | 37.4 | 54.1 | 36.4 |
| 3 | 2 | 1 | 48.4 | 25.4 | 38.2 | 53.0 | 36.0 |
| 10 | 5 | 1 | 48.0 | 25.8 | 37.9 | 52.8 | 35.0 |

such as shown in Fig. 1c. Detection of these objects suffers from both imprecise annotation and inaccurate object localization.

3. Model Dissection

Along with the remarkable progress in object detection, a large number of new methods is published to continuously advance object detection. Newly proposed methods are usually introduced with modifications to the baselines and their ablation validations are conducted with various experiments. The variety makes the key insights ambiguous for the community to appropriately design model architectures for practical situations, e.g., slender object detection.

To avoid this ambiguity and provide a guidance for the detection of slender objects and beyond, we conduct systematic evaluation and analysis in this section. First, we devise a descriptive framework that depicts typical CNN-based object detection in a unified way. Under the framework, the differences of the methods in different paradigms are revealed and can be dissected for detailed comparison with experimental variety well controlled.

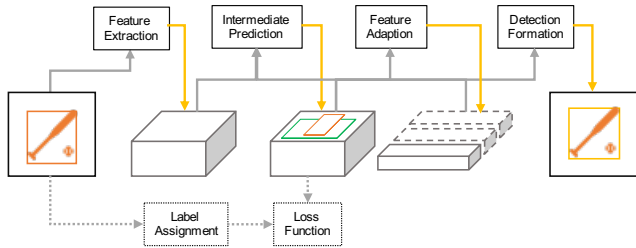


Figure 5: Illustration of the decomposed stages of object detection. Note that a given stage can be performed more than once to form the actual pipeline in certain detectors.

3.1. Standard Object Detection Stages

Basically, the task of object detection is composed of two subtasks, localization and classification. A typical detection method localizes and classifies object regions from rich feature maps extracted by convolutional neural networks in pyramid resolutions. Some of the existing methods [21, 20] directly perform localization and classification on extracted features, and other groups of methods apply feature adaption, e.g. ROI Pooling [22], according to coarsely localized object proposals. They are also referred to as one-stage and two-stage methods in some literature, respectively. For dense detection, post-processing such as redundancy removal is required for most detectors, after which a set of final object detection is formed.

Deriving from the existing methods, four standard stages of object detection can be defined as follows.

1. **Feature Extraction** (\mathcal{FE}) extracts features from the input image to form a high dimensional representation. As deep CNNs [9, 30] and their variants [17] significantly improve the capability of detectors [15, 4], experimental comparison is usually conducted on the same backbones.
2. **Intermediate Prediction** (\mathcal{IP}) localizes and/or classifies object regions. They can be assembled together or performed separately. Researchers have developed different paradigms for localization in recent works, where it can be modeled as a regression problem [18] or a verification problem [15].
3. **Feature Adaption** (\mathcal{FA}) adapts feature maps using intermediate localization results or directly from features for refined prediction. It usually exploits coarse estimation of object regions, i.e. proposals [6], as regions of interest to concentrate on objects for refining classification and localization. Note both \mathcal{FA} and \mathcal{IP} can be utilized multiple times [2].
4. **Detection Formation** (\mathcal{DF}) forms the final results by removing redundant predictions, filtering low-confidence objects, etc. A common detection formation for object detection is non-maximum suppression

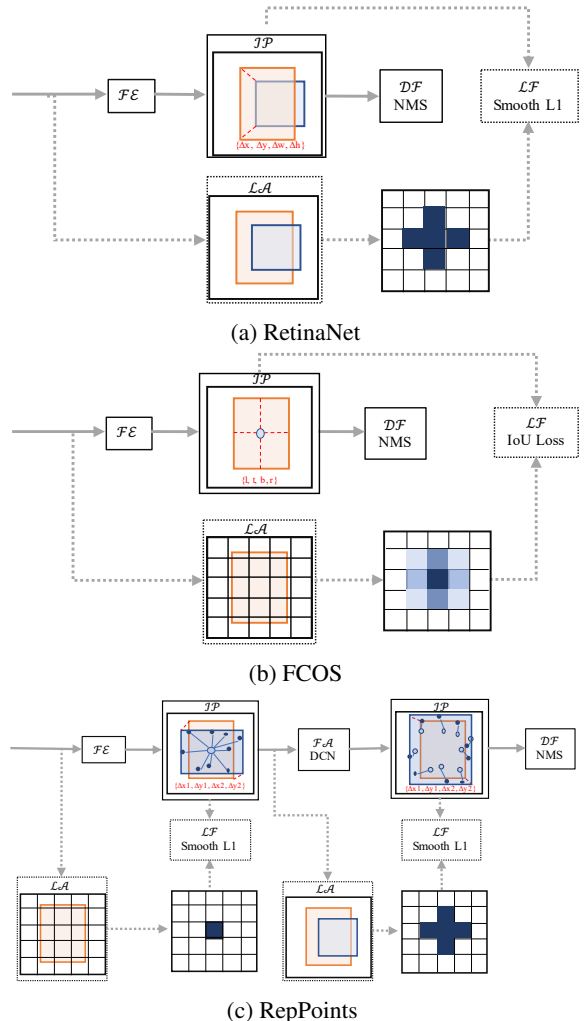


Figure 6: Pipelines of methods whose components are inspected. The stages are introduced in Sec. 3.1. Dotted boxes and arrows indicate the components only used for training.

(NMS) and its successors. Recently, [3] propose end-to-end prediction of object localization and classes, resulting in simplified detection formation.

In addition to these stages that are required for both training and inference, there are options for different training strategies. Typically label assignment and loss function identify the criterion for the training procedure. **Loss Function** (\mathcal{LF}) acts as the optimization target during the training of detectors. It consists of the loss function for classification, where focal loss is dominant, and the loss function for localization, where smooth l1 loss and gIoU loss are preferred choices. **Label Assignment** (\mathcal{LA}) fills the gap between the optimization target and network outputs. It assigns labels to prediction results, making the model trainable. Label assignment is still under active investigation as it is related to localization and classification representation of objects.

3.2. Component Inspection

Under this framework, we are able to rigorously inspect long-existing controversies in object detection in consideration of slender objects. Due to the notable research efforts paid to two-stage methods, we specifically inspect two long-standing controversies in one-stage detectors that receive much attention in recent works.

3.2.1 Anchors versus Anchor-Free

Anchors are central to many detection systems [20, 21] and enable detectors to detect multiple objects at the same location. However, as shown in Sec 2.3, the sub-optimal label assignment based on anchors and IoU matching causes major errors in slender object detection. This drawback may be partly alleviated by specially designed anchor ratios, but this strategy is sensitive to specific data and hyperparameters. Anchor-free detectors [12, 15] provide an alternative approach that directly regresses boxes from point locations instead of anchors. This family of detection methods achieve notable success but their properties remains unclear compared with anchors. Through our inspection on two classical detectors, FCOS [26] and RetinaNet [18], which share a similar pipeline, we manage to reveal the key role of anchors. It provides a proper criterion to select foreground locations where the detection is performed from the background, while the difference in the regression space is proven inconsequential to detection effectiveness.

The two methods are described by our framework in Fig. 6a and Fig. 6b, respectively. As can be seen from Tab. 3, FCOS shows advantages in the overall mAP, which mainly benefits from the improvement on regular objects, but staggers in slender object detection. We conjecture the reason as two-fold. First, slender objects tend to be more dense, leading to more overlapped instances that a single prediction at each location theoretically can not handle. Second, the key component of FCOS improves regular object detection more significantly than slender objects. In the following, we elaborate this in detail by dissecting its components.

Regarding FCOS, there are multiple evolutions in implementation and model design in the derivation from its baseline RetinaNet. Excluding implementation details, differences exist in \mathcal{LF} , \mathcal{LA} , and regression spaces in \mathcal{IP} . More formally, FCOS (A) assigns locations inside object boxes as positive, (B) regresses bounding boxes instead of anchors, (C) uses IoU loss as localization target, and (D) adopts centerness score to re-weight loss and score at different positions. Our model dissection discretely considers the evolutions and inspects the performance changes in slender object detection. Evaluation results are shown in Tab. 3.

With the removal of anchor-based assignment, the performance in all metrics dramatically drops, although the re-

Table 3: Model dissection experiments. Modifications from A to H are explained in Sec 3.2, and a lookup table is provided in appendix. RetinaNet with A-D and FCOS are common in components but bear differences in hyperparameters.

| baseline | w/ | COCO ⁺ mAR | | | COCO mAP | |
|-----------|-----|-----------------------|------|------|----------|------|
| | | all | XS | S | | R |
| RetinaNet | - | 48.4 | 23.4 | 37.8 | 53.9 | 36.4 |
| RetinaNet | A | 37.2 | 15.0 | 26.6 | 42.3 | 30.4 |
| RetinaNet | A-B | 43.6 | 18.6 | 33.1 | 49.3 | 32.2 |
| RetinaNet | A-C | 46.2 | 21.0 | 35.8 | 51.6 | 33.7 |
| RetinaNet | A-D | 48.8 | 22.4 | 37.9 | 54.2 | 37.4 |
| FCOS | A-D | 48.7 | 23.2 | 37.9 | 54.4 | 37.6 |
| RetinaNet | E | 46.6 | 20.7 | 35.7 | 51.6 | 33.5 |
| RetinaNet | E-F | 42.5 | 22.5 | 33.2 | 46.9 | 32.1 |
| RetinaNet | E-G | 42.2 | 19.6 | 33.0 | 46.6 | 32.1 |
| RetinaNet | E-H | 46.5 | 25.3 | 37.4 | 50.7 | 38.0 |
| RepPoints | E-H | 47.0 | 26.2 | 38.1 | 51.0 | 38.4 |

gression is performed basing on anchors. This dissected comparison reveals the major effect of anchors, i.e., a reasonable label assignment strategy properly filters locations suitable for detection, instead of the regression space alone. Other alternations proposed by FCOS gradually fill up the drop, but the improvement is less significant on slender objects. Fundamentally, the proposed exponential offsets regression, which estimates the distance from a point inside bounding boxes to the borders, improves the localization results. The observed improvement supports the conclusion that manually designed anchors are not preferred in terms of the regression space.

IoU loss brings more performance gain in our experiments than reported by [18] and [23]. It identifies another appropriate property of FCOS regression that makes it suitable for IoU loss. Because the regression strategy guarantees that the predicted boxes overlap with the ground truth box, the vanilla IoU loss is always able to optimize in FCOS. However, the overall performance is still below the baseline of RetinaNet because of the massive number of low-quality localizations from the border areas of the bounding boxes. Therefore, the center prior (D in Tab. 3) is introduced to suppress the predictions far from the object centers by re-weighting positive samples. It works well in most cases and substantially improves the detection precision, but is less effective for slender objects whose centers are occluded more often.

3.2.2 Bounding Box and Point Sets

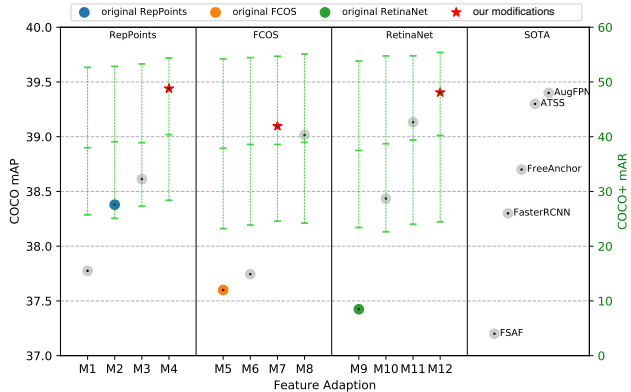
In addition to the anchors, box representation is another active field where much effort [15, 32] has been paid to im-

prove the form of network prediction to fit objects. Rather than the regression space, these methods modify the regression targets. Among the research in this direction, RepPoints [32] stands out due to its promising improvement and novel box representation. It turns box representation into a set of points, specifically 9 points in their experiments, which forms a pseudo box using simple processing such as min-max. Furthermore, the 9-point representation coordinates with Deformable Convolution (DCN) by forming its offsets. Following the proposed \mathcal{FA} layer, an extra \mathcal{IP} stage is performed to refine the initial localization results. The detection procedure of RepPoints is shown in Fig. 6c.

Our experiments validate the remarkable performance of RepPoints and find it advantageous in detecting slender objects. Furthermore, we recognize the supervised \mathcal{FA} as the key process that brings improvements for slender object detection. The dissection also reveals that the conventional 2-point representation can perform comparably or better than the 9-point representation. This conclusion deviates from the ablation study in [32], due to the different implementations of the 2-point representation. In Sec 4.1, we provide the corresponding ablation experiments.

To dissect what forms RepPoints from RetinaNet, we consider the following modifications: (\mathbb{E}) label assignment by assigning the nearest location to box centers as positive; (\mathbb{F}) 2-point representation instead of anchor-based representation; (\mathbb{G}) 9-point representation and corresponding pseudo box formation; and (\mathbb{H}) supervised feature adaption integrating initial localization results with DCNs. The starting point of the dissection of RepPoints, where the \mathcal{LA} stage is replaced by nearest-point assignment, performs better than that of FCOS. The initial label assignment of RepPoints is thus proven a more reasonable strategy. We then change the box representation to a 2-point representation and 9-point representation, referring to RetinaNet with \mathbb{F} and \mathbb{G} in Tab. 3.

In the comparison of “ \mathbb{E} - \mathbb{F} ” and “ \mathbb{E} - \mathbb{G} ” in Tab. 3, the 2-point representation appears even more competitive. This conclusion is further validated by the experiments in Sec. 4.1. What truly makes RepPoints better, for both regular object and slender objects, is the supervised feature adaption. It builds an initial \mathcal{IP} stage that performs rough localization and is used as the offsets of DCNs to refine features. It dramatically enhances RepPoints, especially with a notable advantage on slender objects. Despite the remarkable improvement of supervised feature adaption, which is demonstrated by around 6% in COCO mAP and slender mAR, the insight behind remains opaque. We temporarily shelf this problem and later reveal its detailed properties with module combination experiments at a broader scope.



| # | baseline | modules | mAP | mAR(XS) |
|------|-----------|------------------------------------|-------------|-------------|
| M1 | RepPoints | $\mathbb{I}+\mathbb{L}$ | 37.9 | 24.9 |
| M2* | RepPoints | $\mathbb{I}+\mathbb{J}+\mathbb{L}$ | 38.4 | 25.1 |
| M3 | RepPoints | $\mathbb{I}+\mathbb{J}$ | 38.7 | 27.6 |
| M4† | RepPoints | $\mathbb{I}+\mathbb{K}$ | 39.4 | 28.4 |
| M5* | FCOS | - | 37.6 | 23.2 |
| M6 | FCOS | \mathbb{I} | 37.7 | 23.9 |
| M7 | FCOS | $\mathbb{I}+\mathbb{J}$ | 39.1 | 24.6 |
| M8† | FCOS | $\mathbb{I}+\mathbb{K}$ | 39.0 | 24.2 |
| M9* | RetinaNet | - | 37.4 | 23.4 |
| M10 | RetinaNet | \mathbb{I} | 38.4 | 24.2 |
| M11 | RetinaNet | $\mathbb{I}+\mathbb{J}$ | 39.1 | 24.3 |
| M12† | RetinaNet | $\mathbb{I}+\mathbb{K}$ | 39.4 | 24.4 |

Figure 7: Feature adaption experiments. Modifications \mathbb{I} to \mathbb{L} are introduced in Sec. 4.1, and the original and our improved versions of the mentioned methods are marked with * and †, respectively. The mAP and mAR (XS) are evaluated on COCO and COCO+, where XS stands for extra slender objects. Detailed mAR on COCO+ is shown with green plots in the figure above, corresponding to R, S, and XS mAR from the top to bottom in each column.

4. Improving Slender Object Detection

From Sec 3.2, we reveal the critical components that maintain advantages in detecting slender objects: center prior from FCOS and supervised feature adaption from RepPoints. On the other hand, inspections also reveal ambiguities in understanding the effects of these modules. First, the supervised feature adaption is composed of an intermediate localization stage that accordingly constrains the offsets of DCN. Since it refines the feature and also serves as the basis of the final prediction, the necessity is ambiguous. Second, the center prior is observed less effective on slender objects, indicating the need for an alternative. In this section, we address these issues by delving their properties in depth.

4.1. Self-Adaptation of Features

Promising advantages of RepPoints on slender objects are demonstrated in our previous experiments, where the



(a) convolution (b) reppoints[32] (c) self-adaption

Figure 8: Visualization of different feature adaption strategies. The sampling points are marked as red points relative to the green points. Self-adaption is a generalization of reppoints [32]. (See more details in Sec. 4.1)

supervised feature adaption is identified as the key factor. To further advance slender object detection, we generalize it to a self-adaptation feature adaption, namely self-adaption. The generalized adaption strategy is suitable for other methods as well and can be used as a convenient plug-in. Instead of manually guided restrictions, self-adaption generates offsets of DCNs from features without direct supervision. The intermediate localization is kept but decomposed from the feature adaption. As visualized in Fig. 8, by forcing the sampling points to concentrate on the foreground of objects and to avoid the interference of background, self-adaption brings consistent improvement to detection accuracy for both slender and regular objects. Next, we provide details about the self-adaption through dissection and experiments.

Following the concept of model dissection, we focus on the supervised feature adaption from Sec. 3.2 and its ablations into the following modules to find optimal feature adaption: (I) an initial localization in addition to the final results presented by RepPoints; (J) constraining offsets of DCN using the initial object localization; (K) offsets adaptively learned from the features; and (L) a residual-manner final localization that infers upon the initial localization. Modules (I) and (L) follow the design of RepPoints. To make feature adaption feasible for other existing methods, we use the 2-point representation in Sec.3.2 since the descriptive capacity of the 2-point representation is proven comparably powerful. (K) initially serves as the ablation of (J), but is proven even more effective than the directly supervised version, thus becoming the key concept of self-adaption. The experiments validate it is sufficient to provide guidance for feature adaption without manual restrictions.

Our experimental results for verifying the proposed self-adaption modules are shown in Fig. 7. With self-adaption, all the implemented baselines can be elevated to match or surpass the state of the art, including one-stage and two-stage methods. Note the proposed self-adaption is a compatible component that can be plugged into any other state of the art methods with a negligible computational cost. What we like more about self-adaption is that it achieves notable advantages in slender object detection. It is perfectly suitable for the modified detection paradigm of RepPoints, which is found the most favorable in sole slender evalua-

Table 4: Validation of the slenderness prior. \mathcal{FA} is module \mathbb{K} presented in Sec. 4.1, and SP is short for slenderness prior.

| baseline | \mathcal{FA} | SP | COCO+ mAR | | | | COCO mAP |
|----------|----------------|----|-----------|------|------|------|----------|
| | | | all | XS | S | R | |
| FCOS | | | 48.9 | 23.9 | 38.6 | 54.5 | 37.7 |
| FCOS | ✓ | | 49.4 | 24.2 | 39.0 | 55.1 | 39.0 |
| FCOS | ✓ | ✓ | 49.7 | 26.3 | 40.0 | 54.2 | 38.4 |

tion in Sec. 3.2, and improves the already strong baseline by more than 3% mAR. The gap between regular and slender objects also decreases significantly.

4.2. Slenderness Prior

From the in-depth diagnoses of anchors and anchor-free detection, we conclude that the center prior is crucial for effective anchor-free detection. However, Tab. 3 also shows it is sub-optimal in detecting slender objects. Center prior suppresses spurious prediction that is distant from the object centers by re-weighting using centerness scores defined by

$$centerness = \left(\frac{\min(l, r)}{\max(l, r)} \times \frac{\min(t, b)}{\max(t, b)} \right)^{\frac{1}{2}}. \quad (2)$$

l, r, t, b are the distance to the left, right, top, and bottom border of the bounding box, respectively. With the geometric mean, the decay is slower on the long sides of slender objects but faster on the short sides, causing insufficient training of locating slender objects. Naturally, we extend the formula to

$$centerness^* = \left(\frac{\min(l, r)}{\max(l, r)} \times \frac{\min(t, b)}{\max(t, b)} \right)^s, \quad (3)$$

where s is the slenderness of objects. It favors slender objects that are challenging for precise detection and fasten the score decay of regular objects.

To validate the effectiveness of slenderness prior, we perform experiments using the baseline model of FCOS (M5) and its variant with self-adaption (M8) introduced in Sec. 4.1. As the results in Tab. 4 demonstrate, this natural extension significantly improves the detection mAR for slender objects, with an acceptable sacrifice of the mAP for R objects. Despite an mAR degradation for R objects, the mAR of XS and S improve 2.1% and 1.0%, respectively. It indicates that the slenderness prior is a favorable trade-off between slender and regular objects, as the overall mAR reaches 49.7%.

5. Conclusion

In this paper, we investigate an important yet long-overlooked problem of slender object detection. A comprehensive framework is established for dissecting and comparing different object detection methods as well as their components and variants. Based on this framework, a series

Table 5: Lookup table for our model assessment.

| # | Stage | Description | Reference |
|---|------------------------------|--|--------------------------------|
| A | $\mathcal{L}A$ | Assign in-object locations as positive | FCOS [26] |
| B | $\mathcal{I}P$ | Regression from object center | FCOS [26] |
| C | $\mathcal{L}F$ | IoU Los | IoUNet [13], FCOS [26] |
| D | $\mathcal{L}A, \mathcal{D}F$ | Center-prior | FCOS [26] |
| E | $\mathcal{L}A$ | Assign object center as positive | RepPoints [32] |
| F | $\mathcal{I}P$ | 2-point box representation | RetinaNet [18], RepPoints [32] |
| G | $\mathcal{I}P$ | 9-point box representation | RepPoints [32] |
| H | $\mathcal{F}A$ | Supervised feature adaptation | RepPoints [32] |
| I | $\mathcal{F}A$ | Initial localization prediction | RepPoints [32] |
| J | $\mathcal{F}A$ | Supervised DCN | RepPoints [32] |
| K | $\mathcal{F}A$ | Self-adaptation of features | - |
| L | $\mathcal{I}P$ | Residual localization prediction | RepPoints [32] |

of key observations and insights is obtained. Furthermore, we have proposed two effective strategies for significantly improving the performance of slender object detection.

Acknowledgment

The authors would like to thank Prof. Xiang Bai for insightful discussion.

Appendix

A. Modifications Lookup Table

To help understand the various experiment inconsistency we address in this paper, we prove a lookup table for the ablation modifications involved in the paper in Tab. 5.

B. Evaluation Metrics

As mentioned in our paper, the task of object detection is composed of the object localization and classification. The evaluation metrics is supposed to correspondingly address them. Precision and recall are introduced into object detection to measure the effectiveness. In the field of detection, localization results with correct classification and intersection over union (IoU) above discrete thresholds are counted as true positive, while others are regarded as the false. Then the precision and recall are computed according to the formula shown in Fig. 9.

Using the definition of “precision” and “recall”, the precision-recall curve can be obtained to compute the average precision (AP). Namely, the AP score for a specific category is the average of precision over a set of recalls,

as the recall scores are typically inversely related to the precision scores. The terms “mean” and “average” in mean average recall (mAP) indicates the mean over categories, recall scores, and IoU scores. As shown in Fig. 9, the number of total positives is required for computing the AP scores

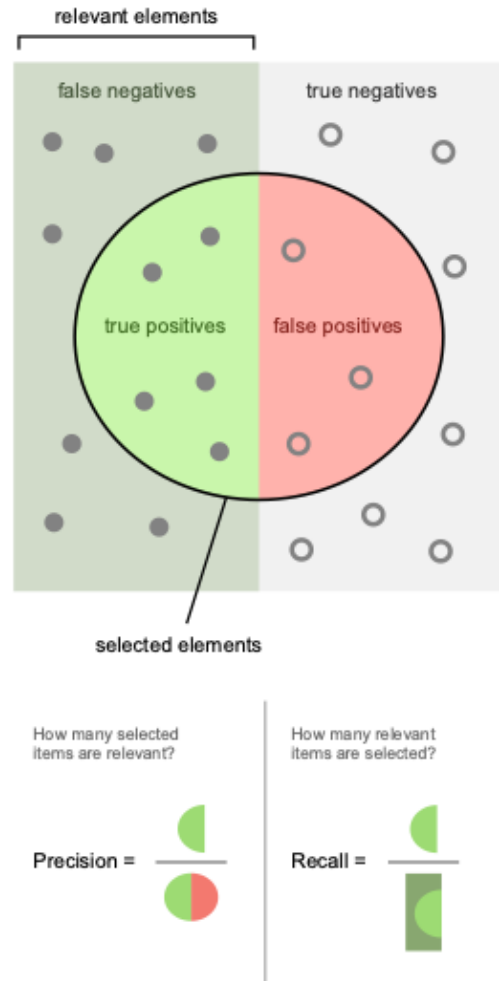


Figure 9: Precision and recall [28].



Figure 10: Pseudo masks generated by Cascaded RCNN [2] for $COCO^+$. The boxes are the ground-truth labels and the masks are accordingly generated. Only masks for slender objects are visualized.

for a particular group of objects. However, it is inestimable due to the representation of predicted boxes. Thus for the compatibility with existing object detection methods, we use mean average recall (mAR) to avoid the deviation. We define mAR as the the mean average recall over IoU thresholds from 0.5 to 0.95 with a 0.05 interval and object categories. In consideration of detection precision, the amount of detection in an image is limited by a specific number, 100 in our experiments.

C. Pseudo Mask Generation

We use images containing slender objects from Objects365 [25] Dataset to complement COCO. As there are 365 different categories in Objects365, we map objects categories that appear in COCO into the $COCO^+$ dataset to be mixed with the original COCO.

For slenderness estimation, we use a top-performance instance segmentation model from Detectron2 [29], an implementation of [2] with a ResNeXt152 backbone. Benefiting from the pre-trained models of Detectron2, we do not need to re-train the segmentation model. We use no test time augmentation during inference, and the resolution of the input images during testing is fixed to (800, 1333). As mentioned in Section 2.2 in our paper, the ground truth bounding boxes are used as proposals while generating the masks. Consequently, the produced pseudo masks are accurate enough and reliable to measure the slenderness of objects. Some examples of the generated pseudo masks of slender objects are shown in Figure. 10.

We have submitted the generated annotation file for the validation set of $COCO^+$ in the “data and code” section, which refers to the same image files from COCO and Objects365.

References

- [1] Yancheng Bai, Yongqiang Zhang, Mingli Ding, and Bernard Ghanem. Sod-mtgan: Small object detection via multi-task generative adversarial network. In *ECCV*, pages 206–221, 2018. 1
- [2] Zhaowei Cai and Nuno Vasconcelos. Cascade r-cnn: Delving into high quality object detection. In *Proceedings of the IEEE conference on computer vision and pattern recognition*, pages 6154–6162, 2018. 1, 3, 5, 10
- [3] Nicolas Carion, Francisco Massa, Gabriel Synnaeve, Nicolas Usunier, Alexander Kirillov, and Sergey Zagoruyko. End-to-end object detection with transformers. In *arXiv preprint arXiv:2005.12872*, 2020. 5
- [4] Kaiwen Duan, Song Bai, Lingxi Xie, Honggang Qi, Qingming Huang, and Qi Tian. Centernet: Keypoint triplets for object detection. In *Proceedings of the IEEE/CVF International Conference on Computer Vision (ICCV)*, October 2019. 5
- [5] Peter R Florence, Lucas Manuelli, and Russ Tedrake. Dense object nets: Learning dense visual object descriptors by and for robotic manipulation. In *Conference on Robot Learning*, pages 373–385, 2018. 1
- [6] Ross Girshick, Jeff Donahue, Trevor Darrell, and Jitendra Malik. Rich feature hierarchies for accurate object detection and semantic segmentation. In *Proceedings of the IEEE Conference on Computer Vision and Pattern Recognition (CVPR)*, June 2014. 1, 5
- [7] Chaoxu Guo, Bin Fan, Qian Zhang, Shiming Xiang, and Chunhong Pan. Augfpn: Improving multi-scale feature learning for object detection. In *CVPR*, pages 12595–12604, 2020. 1
- [8] Kaiming He, Ross Girshick, and Piotr Dollár. Rethinking imagenet pre-training. In *ICCV*, pages 4918–4927, 2019. 1
- [9] Kaiming He, Xiangyu Zhang, Shaoqing Ren, and Jian Sun. Deep residual learning for image recognition. In *CVPR*, pages 770–778, 2016. 4, 5
- [10] Derek Hoiem, Yodsawalai Chodpathumwan, and Qieyun Dai. Diagnosing error in object detectors. In *European conference on computer vision*, pages 340–353. Springer, 2012. 1
- [11] Han Hu, Jiayuan Gu, Zheng Zhang, Jifeng Dai, and Yichen Wei. Relation networks for object detection. In *CVPR*, pages 3588–3597, 2018. 1
- [12] Lichao Huang, Yi Yang, Yafeng Deng, and Yinan Yu. Densebox: Unifying landmark localization with end to end object detection. *arXiv preprint arXiv:1509.04874*, 2015. 1, 6
- [13] Borui Jiang, Ruixuan Luo, Jiayuan Mao, Tete Xiao, and Yunying Jiang. Acquisition of localization confidence for accurate object detection. In *Proceedings of the European Conference on Computer Vision (ECCV)*, pages 784–799, 2018. 9
- [14] Licheng Jiao, Fan Zhang, Fang Liu, Shuyuan Yang, Lingling Li, Zhixi Feng, and Rong Qu. A survey of deep learning-based object detection. *IEEE Access*, 7:128837–128868, 2019. 1
- [15] Hei Law and Jia Deng. Cornernet: Detecting objects as paired keypoints. In *Proceedings of the European Conference on Computer Vision (ECCV)*, September 2018. 5, 6

- [16] Minghui Liao, Zhaoyi Wan, Cong Yao, Kai Chen, and Xiang Bai. Real-time scene text detection with differentiable binarization. In *AAAI*, pages 11474–11481, 2020. **1**
- [17] Tsung-Yi Lin, Piotr Dollár, Ross Girshick, Kaiming He, Bharath Hariharan, and Serge Belongie. Feature pyramid networks for object detection. In *CVPR*, pages 2117–2125, 2017. **4, 5**
- [18] Tsung-Yi Lin, Priya Goyal, Ross Girshick, Kaiming He, and Piotr Dollár. Focal loss for dense object detection. In *Proceedings of the IEEE international conference on computer vision*, pages 2980–2988, 2017. **1, 4, 5, 6, 9**
- [19] Tsung-Yi Lin, Michael Maire, Serge Belongie, James Hays, Pietro Perona, Deva Ramanan, Piotr Dollár, and C Lawrence Zitnick. Microsoft coco: Common objects in context. In *European conference on computer vision*, pages 740–755. Springer, 2014. **3**
- [20] Wei Liu, Dragomir Anguelov, Dumitru Erhan, Christian Szegedy, Scott Reed, Cheng-Yang Fu, and Alexander C Berg. Ssd: Single shot multibox detector. In *ECCV*, pages 21–37. Springer, 2016. **5, 6**
- [21] Joseph Redmon, Santosh Divvala, Ross Girshick, and Ali Farhadi. You only look once: Unified, real-time object detection. In *CVPR*, pages 779–788, 2016. **1, 5, 6**
- [22] Shaoqing Ren, Kaiming He, Ross Girshick, and Jian Sun. Faster r-cnn: Towards real-time object detection with region proposal networks. In C. Cortes, N. D. Lawrence, D. D. Lee, M. Sugiyama, and R. Garnett, editors, *Advances in Neural Information Processing Systems 28*, pages 91–99. Curran Associates, Inc., 2015. **1, 5**
- [23] Hamid Rezaatofghi, Nathan Tsoi, JunYoung Gwak, Amir Sadeghian, Ian Reid, and Silvio Savarese. Generalized intersection over union: A metric and a loss for bounding box regression. In *CVPR*, pages 658–666, 2019. **6**
- [24] Igor Ševo and Aleksej Avramović. Convolutional neural network based automatic object detection on aerial images. *IEEE geoscience and remote sensing letters*, 13(5):740–744, 2016. **1**
- [25] Shuai Shao, Zeming Li, Tianyuan Zhang, Chao Peng, Gang Yu, Xiangyu Zhang, Jing Li, and Jian Sun. Objects365: A large-scale, high-quality dataset for object detection. In *Proceedings of the IEEE international conference on computer vision*, pages 8430–8439, 2019. **3, 10**
- [26] Zhi Tian, Chunhua Shen, Hao Chen, and Tong He. Fcos: Fully convolutional one-stage object detection. In *ICCV*, pages 9627–9636, 2019. **2, 6, 9**
- [27] Konstantinos Topouzelis, Apostolos Papakonstantinou, and Shungudzemwoyo P Garaba. Detection of floating plastics from satellite and unmanned aerial systems (plastic litter project 2018). *International Journal of Applied Earth Observation and Geoinformation*, 79:175–183, 2019. **1**
- [28] Wikipedia contributors. Precision and recall — Wikipedia, the free encyclopedia, 2020. [Online; accessed 16-September-2020]. **9**
- [29] Yuxin Wu, Alexander Kirillov, Francisco Massa, Wan-Yen Lo, and Ross Girshick. Detectron2. <https://github.com/facebookresearch/detectron2>, 2019. **10**
- [30] Saining Xie, Ross Girshick, Piotr Dollár, Zhuowen Tu, and Kaiming He. Aggregated residual transformations for deep neural networks. In *CVPR*, pages 1492–1500, 2017. **3, 5**
- [31] Shuo Yang, Ping Luo, Chen-Change Loy, and Xiaoou Tang. Wider face: A face detection benchmark. In *Proceedings of the IEEE Conference on Computer Vision and Pattern Recognition (CVPR)*, June 2016. **1**
- [32] Ze Yang, Shaohui Liu, Han Hu, Liwei Wang, and Stephen Lin. Reppoints: Point set representation for object detection. In *Proceedings of the IEEE International Conference on Computer Vision*, pages 9657–9666, 2019. **6, 7, 8, 9**
- [33] Peng Zhou, Bingbing Ni, Cong Geng, Jianguo Hu, and Yi Xu. Scale-transferrable object detection. In *CVPR*, pages 528–537, 2018. **1**
- [34] Barret Zoph, Ekin D Cubuk, Golnaz Ghiasi, Tsung-Yi Lin, Jonathon Shlens, and Quoc V Le. Learning data augmentation strategies for object detection. *arXiv preprint arXiv:1906.11172*, 2019. **1**